New Insights into the Bonding Properties of $[Ag_{25}(SR)_{18}]^-$ Nanoclusters from X-ray Absorption Spectroscopy

Ziyi Chen[†], Andrew G. Walsh[†], Xiao Wei[‡], Manzhou Zhu[‡], Peng Zhang[,†]*

[†] Department of Chemistry, Dalhousie University, Halifax, Nova Scotia, B3H 4R2, Canada

[‡] Department of Chemistry and Center for Atomic Engineering of Advanced Materials, Institute of Physical Science and Information Technology and AnHui Province Key Laboratory of Chemistry for Inorganic/Organic Hybrid Functionalized Materials, Anhui University, Hefei, Anhui 230601, P.R. China

Corresponding Author

E-mail: peng.zhang@dal.ca

KEYWORDS

silver nanoclusters, $Ag_{25}(SR)_{18}$, extended X-ray absorption fine structure (EXAFS), bonding properties

ABSTRACT

Atomically precise metal nanoclusters have attracted significant interest due to their molecule-like properties. $[Ag_{25}(SR)_{18}]^-$ is one of the Ag nanoclusters having a unique structure similar to its Au counterpart but different from most other Ag nanoclusters. In this study, a new five-shell fitting method was developed to analyze the extended X-ray absorption fine structure (EXAFS) spectra of $[Ag_{25}(SR)_{18}]^-$ to provide more insights into its bonding properties. This new method was successfully applied to compare the bond lengths as the temperature changed from 300 K to 90 K. Interestingly, the metal core of $[Ag_{25}(SR)_{18}]^-$ shows negative thermal expansion behaviour that is not observed for $Au_{25}(SR)_{18}$. These unique bonding properties of $[Ag_{25}(SR)_{18}]^-$ could be related to the Ag_4 tetrahedral units found in the metal core, which are absent in $Au_{25}(SR)_{18}$. These new findings about its bonding properties can provide a better understanding of the structure-property relationship of $[Ag_{25}(SR)_{18}]^-$. This new EXAFS analysis method could be applied to gain insights into the bonding properties of other metal nanoclusters.

1. INTRODUCTION

Thiolate-protected metal nanoclusters (NCs) typically are atomically precise, and they can be denoted by exact formulae such as $M_n(SR)_m$, where M is a metal atom and SR is a thiolate ligand.[1] Given their small sizes (less than 2 nm), the surface-to-volume ratio is large, and quantum confinement effects are induced.[2] Thus, these metal nanoclusters have molecular-like behavior and possess unique surface and electronic properties, which are beneficial for various applications in catalysis, sensing, and imaging.[3–8] Due to the increasing interest in thiolate-protected metal nanoclusters, many nanoclusters have been successfully synthesized and characterized. Au and Ag nanoclusters are two major groups in this area. Au nanoclusters are widely studied in terms of their structures, properties and applications.[9] In contrast, Ag nanoclusters are less studied due to their relatively low stability.[10] With the improvement of synthesis methods, synthesizing stable Ag nanoclusters has become easier, and their total structures have been determined such as $Ag_{25}(SPhMe_2)_{18}PPh_4$ (abbreviated as $[Ag_{25}(SR)_{18}]^-$) and $Na_4Ag_{44}(p\text{-MBA})_{30}$.[11,12] The improvement in their stability could be due to their closed-shell electron configuration like noble gas atoms. The $[Ag_{25}(SR)_{18}]^-$ nanocluster has been found to be the only matching analogue with Au nanoclusters. It has an icosahedron Ag_{13} metal core and protected by six Ag_2S_3 staple motifs. The $[Ag_{25}(SR)_{18}]^-$ satisfies a quasi-T_h symmetry. It has eight free electrons with the electron configuration $1S^2|1P^6$.[11]

The study of the properties of these metal nanoclusters is essential for their applications in different areas. X-ray absorption spectroscopy (XAS) is a unique technique that contains both structural and electronic information in one spectrum. XAS has already been applied in the study of many different metal nanoclusters.[13–21] Extended X-ray absorption spectroscopy fine structure (EXAFS) is a part of XAS that provides detailed structural and bonding information of materials

like coordination numbers (CNs), bond distances, and interatomic disorder.[22] It is a useful tool to study the structural changes of materials upon varying external variables such as solvents and temperature.[13,14,23,24] To obtain structural information, the EXAFS spectrum is extracted and converted to k-space, and then Fourier transformed (FT) to its FT-EXAFS spectrum which can be fitted with appropriate fitting models.[25] Finding an appropriate fitting model is the key to obtaining reliable structural information from fitting of a FT-EXAFS spectrum. One important factor to consider for a fitting model is the number of fitting shells. Normally, the fitting shells are distinguished by the different types of bonds. It should be noted that the fitting shell mentioned in this paper is different from the terminology "shell" used in nanocluster chemistry. Herein, we present a novel and more detailed study on the unique bonding properties of $[Ag_{25}(SR)_{18}]^-$ by measuring its Ag K-edge EXAFS at two temperatures: 90 K and 300 K. In particular, a new EXAFS fitting method is introduced by re-defining the number of fitting shells determined by its bond distribution and its wavelet transformation (WT) plot in combination with its simulated spectrum.

2. METHODOLOGY

2.1 Synthesis of Nanoclusters

The detailed synthesis procedure of $[Ag_{25}(SR)_{18}]^-$ nanoclusters has been reported elsewhere.[11] Briefly, 2,4-dimethylbenzenethiol ($HSPhMe_2$) was used as the thiolate ligand. The mixture of $AgNO_3$ and thiolate ligand solution was reduced by $NaBH_4$ in the presence of tetraphenyl phosphonium bromide ($PPh_4^+Br^-$), which was used as counterions. Then, the synthesized sample was purified following the standard procedure.[11]

2.2 XAS Measurements and Fitting Method

The XAS measurements were conducted at the Sector 20-BM beamline of the Advance Photon Source (operating at 7.0 GeV) at Argonne National Labs in Argonne, IL. The Ag K-edge data was collected in fluorescence mode. A Si (111) monochromator crystal with a harmonic rejection mirror was used to select the desired wavelength. The powders of $[Ag_{25}(SR)_{18}]^-$ were sealed in Kapton film pouches and were folded. The foil references were simultaneously measured with each scan for the edge energy calibration. The XAS measurement of $[Ag_{25}(SR)_{18}]^-$ at 90 K was carried out by using a liquid He cryostat. The fitting of the EXAFS spectra were performed using Artemis and Athena.[26] The data collected at 300 K and 90 K were analyzed using k_3-weighting. For the two-shell fitting method, a k-range of 2.8-12.5 $Å^{-1}$ and a fitting window of 1.26-3.0 Å were used for the data collected at 300K, while a k-range of 3-12.8 $Å^{-1}$ and a fitting window of 1.3-3.0 Å were used for the low-temperature data. The same k-ranges were applied for the five-shell fitting method, but wider fitting windows were used (1.05-4.0 Å for 300 K, and 1.0-4.0 Å for 90 K). To reduce the number of variables for multi-shell fitting, all coordination numbers were fixed from the theoretical calculation of the crystal structure. The energy shift (E_0) of all fitting shells were correlated and the Debye-Waller factors (σ^2) for all Ag-Ag shells were correlated. The amplitude reduction factors (S_0^2) for both temperatures were determined from the foil that was measured simultaneously with the samples. They were fixed at 0.90 for both temperatures while performing the FT-EXAFS fitting of the samples.

2.3 EXAFS Simulation and Wavelet Transformed EXAFS

Simulation of the Ag K-edge EXAFS spectrum at 90 K was performed using the FEFF8 program code.[27] In this simulation, only 25 Ag atoms were included without any thiolate ligands. There are three different sites: center, surface, and staple. First, the simulation of the Ag K-edge EXAFS spectrum for each site was done by selecting one atom from different sites as the target

atom. The Debye card was used to account for the temperature effect. The Debye temperature of the pure Ag_{25} cluster without thiolate ligands was calculated to be 196 K using the equation reported in the literature.[28] Then, the simulation of the overall Ag K-edge EXAFS spectrum for the $[Ag_{25}(SR)_{18}]^-$ nanocluster was obtained by weight averaging the y-axis of each site simulation. The weight was calculated by the number of Ag atoms in each site divided by the total number of Ag atoms in the cluster. Wavelet transformations (WTs) of the EXAFS data at low temperature were performed by using the Morlet wave transform.[29] The same k-range of 3.0-12.8 $Å^{-1}$ was used for both the experimental data and the simulated data. First, the wavelet parameters $\eta = 5$ and $\sigma = 1$ were used for the experimental data, which has high resolution in R-space and low resolution in k-space. Then, the wavelet parameters $\eta = 2$ and $\sigma = 1$ were used for both WT plots to obtain high resolution in k-space and low resolution in R-space.

3. RESULTS AND DISCUSSION

The Ag K-edge XAS spectra of $Ag_{25}(SR)_{18}$ were generated using data collected at 300 K and 90 K. As displayed in Figure 1a, there are two major peaks appearing in the FT-EXAFS spectra of the samples. The peak at around 2 Å is due to the Ag-S bond. The other peak at around 2.8 Å originates from the Ag-Ag bond. The spectra were compared with the spectrum of Ag foil. The intensity of the peaks can be related to the size and the Debye-Waller factor of the materials. In Figure 1a, the spectra of $[Ag_{25}(SR)_{18}]^-$ exhibits much lower peak intensities of the Ag-Ag shells than those in the Ag foil spectrum, indicating that the size of $[Ag_{25}(SR)_{18}]^-$ is small. It is interesting that the spectrum of the sample at 90 K shows higher peak intensities than those at 300 K, which can be due to the small Debye-Waller factor and suppression of the thermal fluctuation of chemical bonds at low temperature.[30]

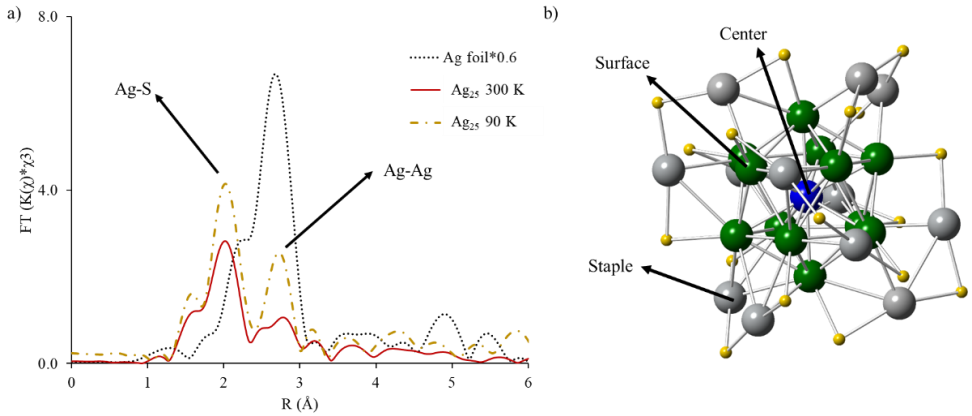

Figure 1. a) Ag K-edge FT-EXAFS spectra of Ag foil and $[Ag_{25}(SR)_{18}]^-$ at 90 K and 300 K. The intensity of the spectrum of Ag foil was multiplied by 0.6. b) The crystal structure of $[Ag_{25}(SR)_{18}]^-$ with indication of different Ag coordination environments (S atoms – yellow; center Ag atom – blue; surface Ag atoms – green; staple Ag atoms – grey).

The analysis of $[Ag_{25}(SR)_{18}]^-$ begins with a two-shell fit for the spectra collected at both temperatures, because there are two major bond interactions in the sample: Ag-S and Ag-Ag. The structural parameters obtained from the fittings are summarized in Table 1. There is a slight decrease in the bond length of Ag-S bonds as the temperature decreases, but the change is only 0.01 Å, which is within the margin of uncertainty. On the other hand, the Ag-Ag bonds show an increase of 0.04 Å upon the temperature reduction, but is still within the margin of uncertainty. The crystal structure of $[Ag_{25}(SR)_{18}]^-$ nanoclusters has been reported previously[11] and is depicted in Figure 1b. It has one center atom and 12 surface atoms that form a 13-atom icosahedral metal core. The remaining 12 Ag atoms are bonded with S atoms to form six staple motifs (Ag_2S_3). Thus, there are three different Ag coordination environments: center, surface, and staple. The two-shell fitting method cannot clearly show the temperature effect on different Ag-Ag bonds. Additionally, the large Debye-Waller factor for the Ag-Ag shell could indicate the great variation among the Ag-Ag bond distances. It is necessary to break down the Ag-Ag shell, so that more precise fitting results can be obtained.

Table 1. EXAFS Two-shell Fitting Results for $[Ag_{25}(SR)_{18}]^-$ NCs at 300 K and 90 K

Temperature	Shell	CN (fixed)	R (Å)	σ^2 (Å^2)	ΔE_0 (eV)	R-factor	Averaged R (Å)[a]
300 K	Ag-S	1.44	2.45 (1)	0.0060 (9)	- 0 (1)	0.0297	2.43
	Ag-Ag	5.60	2.85 (3)	0.029 (3)			2.94
90 K	Ag-S	1.44	2.44 (1)	0.0035 (9)	4 (1)	0.0364	-
	Ag-Ag	5.60	2.89 (2)	0.017 (2)			-

[a] Averaged bond distances calculated from the crystal structure reported in Ref11.

To investigate the number of fitting shells, 2D WT-EXAFS plots were generated. This 2D plot combines the information from FT-EXAFS (R-space) and k-space. The k-space contains the oscillations that are generated by the interactions between target atoms and backscattering atoms.[31] The WT plot has an advantage to show the possible shells that could be missed in a conventional FT-EXAFS spectrum. Figure 2a shows the WT-EXAFS plots of $[Ag_{25}(SR)_{18}]^-$ at 90 K with high resolution in R-space and low resolution in k-space. Here, only the data collected at low temperature was analyzed owing to the low signal-to-noise ratio at 300 K. Moreover, the temperature effect cannot affect the analysis of fitting shells because the number of fitting shells should be only determined by the structure of $[Ag_{25}(SR)_{18}]^-$ but not the temperature. Obviously, there are two domain regions. The bottom region centered at around R ~2 Å corresponds to the Ag-S shell, and the top region centered at around R ~2.8 Å can be assigned to the Ag-Ag shell, which is consistent with the observation of two major peaks from the conventional FT-EXAFS spectrum. The WT-EXAFS plot in Figure 2b displays the experimental data with high resolution in k-space and low resolution in R-space, which can more clearly show how many different shells are present for each peak in the FT-EXAFS spectrum. In this case, Figure 2b shows different distinct areas at high R region. The area around R ~3.5 Å and k ~ 10 Å^{-1} has a doublet.

However, it is difficult to determine whether it is one shell or two shells based on the current resolution of the FT-EXAFS.

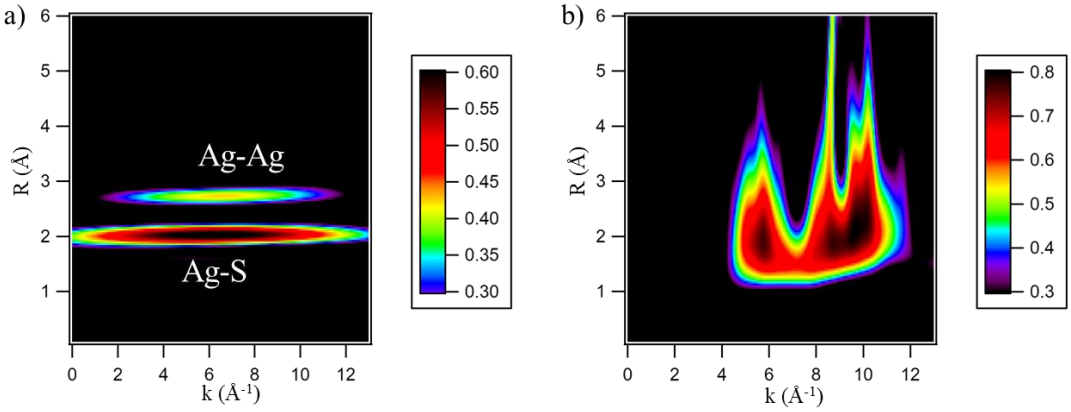

Figure 2. WT-EXAFS map of experimental data collected at 90 K a) with high resolution in R-space and low resolution in k-space, and b) with low resolution in R-space and high resolution in k-space.

The major challenge with the WT-EXAFS plot shown in Figure 2b is that the thiolate ligand effect cannot be excluded. From Figure 2a, it is obvious that the intensity of Ag-S shell is much stronger than that of Ag-Ag shell. This large contribution from the Ag-S shell can affect the shape and areas of the Ag-Ag shell in the WT-EXAFS plot. To solve this problem, a new strategy was developed to carefully remove the ligand effect in the WT-EXAFS plot. The simulated EXAFS spectrum provides flexibility to modify the structural model, so that it is possible to generate an EXAFS spectrum that only has contributions from the Ag-Ag shell. To achieve this, a structural model of $[Ag_{25}(SR)_{18}]^-$ NCs without the thiolate ligands was used to perform the simulation of the Ag K-edge EXAFS spectrum at 90 K, and then this simulated EXAFS spectrum was converted to a WT-EXAFS plots. As shown in Figure 3, the simulated WT-EXAFS plot has a similar domain with the plot of experimental data (R: 1-4 Å, k: 4-11 $Å^{-1}$). It clearly shows that there are four distinct areas at high R region corresponding to four shells of

Ag-Ag bonds. In addition, the color intensity of each shell could be positively related to the number of bonds. Hence, the combination of the simulation of the EXAFS spectrum and its WT-EXAFS plot can prove that there are four different Ag-Ag shells. This new strategy shows the benefits of using simulated WT-EXAFS plots to guide the fitting of FT-EXAFS spectra.

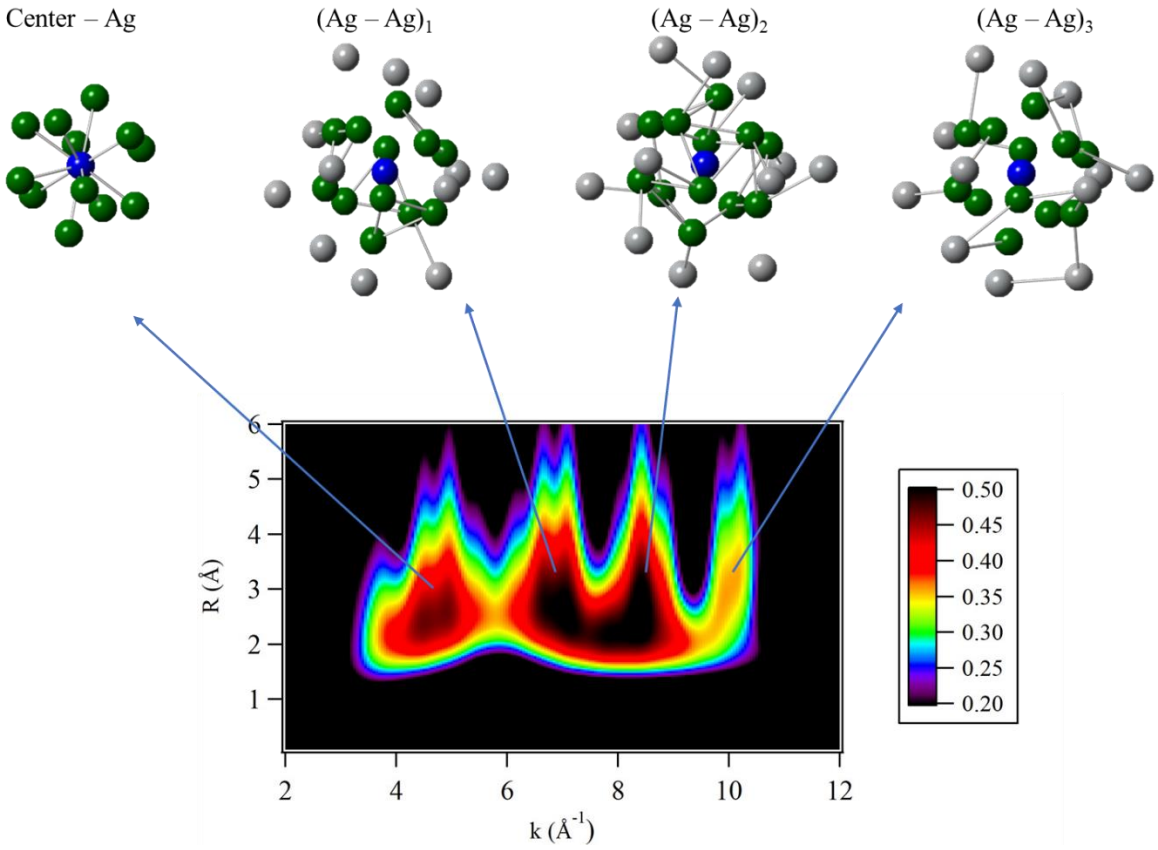

Figure 3. Simulated WT-EXAFS map with only 25 Ag atoms considered. The corresponding bonds involved in each shell are shown in the crystal structures.

To further track the origin of the four Ag-Ag shells in the $[Ag_{25}(SR)_{18}]^-$ nanoclusters uncovered by the WT-EXAFS analysis, the bond distribution of Ag-Ag bonds is plotted. As shown in Figure 3 Figure 4, the first Ag-Ag shell consists only short bonds (~2.76 Å) from the center atom to the surface Ag atoms (center–Ag shell). The second Ag-Ag group ($(Ag\text{-}Ag)_1$ shell) consists of short surface-surface bonds forming triangles that are not located directly beneath the staple

motifs. The $(Ag\text{-}Ag)_1$ shell also includes short surface-staple bonds because of the distortion of some staple Ag atoms. The third Ag-Ag shell, $(Ag\text{-}Ag)_2$, is composed of longer surface-surface bonds and some surface-staple bonds. The fourth Ag-Ag shell, $(Ag\text{-}Ag)_3$, has longer bonds between surface atoms and staple atoms with some interactions between staple atoms. Based on the structure, the averaged coordination numbers and bond distances for each shell were calculated.

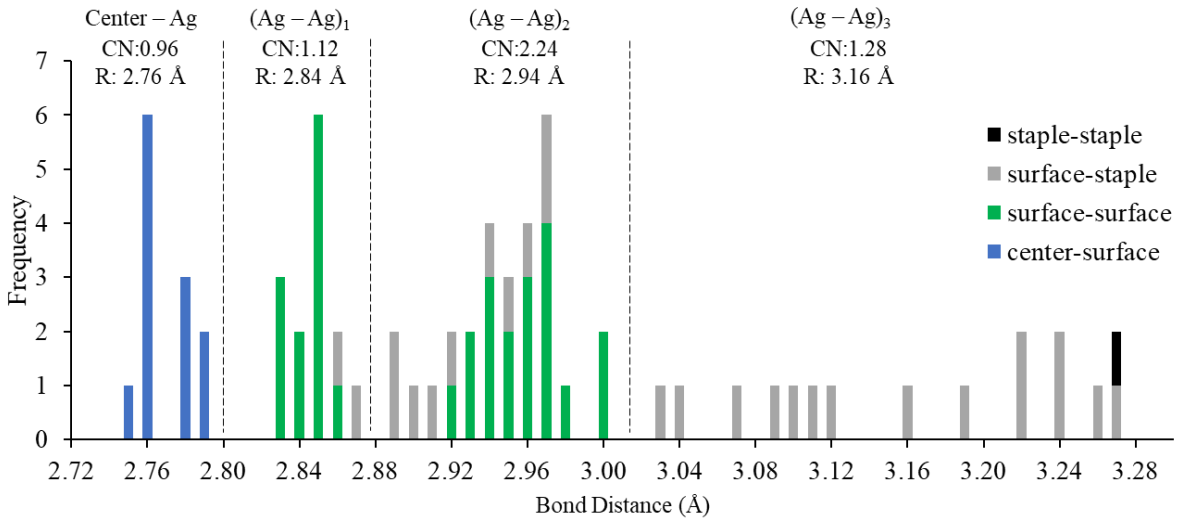

Figure 4. The bond distribution histogram of Ag-Ag bonds in $[Ag_{25}(SR)_{18}]^-$ NCs.

A five-shell fitting method was applied for the $[Ag_{25}(SR)_{18}]^-$ spectra at both 300 K and 90 K. As shown in Figure 5a and b, the five-shell fitting method shows a better match between the experimental FT-EXAFS data and the fitting curve than the two-shell fitting method, particularly for the peak at around 2.8 Å and the small peak at around 3.1 Å, which are two peaks that correspond to Ag-Ag bonds.

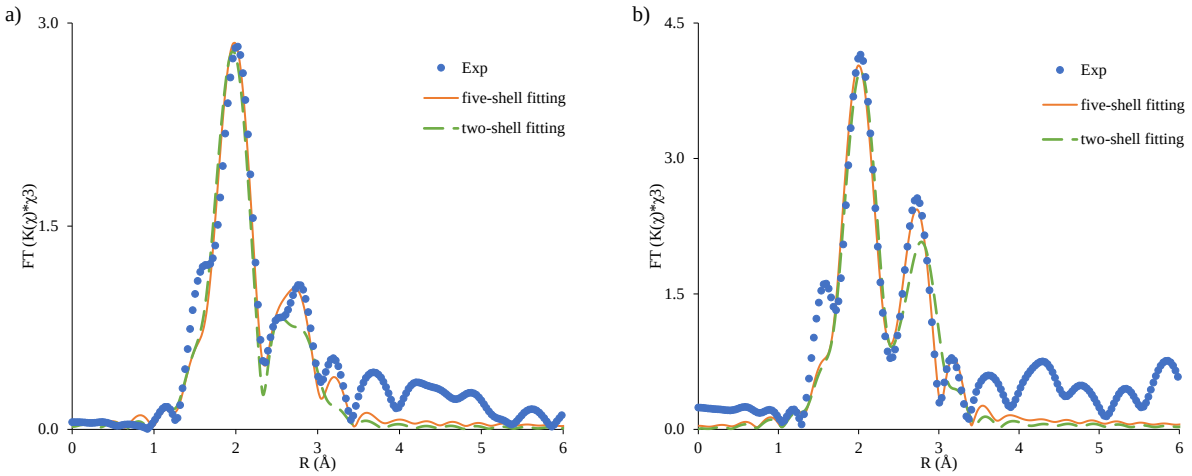

Figure 5. The Ag K-edge FT-EXAFS spectrum of $[Ag_{25}(SR)_{18}]^-$ with five-shell fitting and two-shell fitting at a) 300 K and b) 90 K.

Table 2 summarizes the structural parameters of $[Ag_{25}(SR)_{18}]^-$ obtained from the five-shell fitting of the FT-EXAFS spectra at two temperatures. In general, the bond distances obtained from the fitting results are in good agreement with the calculated average bond lengths from its crystal structure, which can further validate the fitting model. The Debye-Waller factors (σ^2) at 90 K are smaller than those at 300 K. Generally, both static disorder and dynamic disorder can contribute to the Debye-Waller factors.[32] In this case, the difference of Debye-Waller factors between the two temperatures could be largely due to the dynamic disorder. Moreover, the Debye-Waller factors of the Ag-S shell are smaller than those of the Ag-Ag shell at both temperatures. Interestingly, as the temperature decreased, the bond length of Ag-S decreased by about 0.024 Å. This is accompanied by obvious expansions of the center-Ag bonds and $(Ag\text{-}Ag)_1$ bonds, which are increased by about 0.04 Å (still within the margin of uncertainty) and 0.05 Å (outside the margin of uncertainty), respectively. The metal core shows negative thermal expansion, which is not common behavior of metallic materials. Additionally, the increments of Ag-Ag bond length are greater than the decrement of the Ag-S bonds, indicating that the Ag-S bonds are stiffer than the Ag-Ag bonds within $[Ag_{25}(SR)_{18}]^-$.

Table 2. EXAFS Five-shell Fitting Results for $[Ag_{25}(SR)_{18}]^-$ NCs at 300 K and 90 K

Shell	Temperature (K)	R (Å)	σ^2 (Å^2)
Ag – S	300	**2.472 (7)**	0. 0058 (7)
	90	**2.448 (7)**	0.0033 (7)
		2.43[a]	-
Center – Ag	300	**2.74 (3)**	0.011 (2)
	90	**2.78 (3)**	0.007 (3)
		2.76[a]	-
$(Ag – Ag)_1$	300	**2.82 (2)**	0.011 (2)
	90	**2.87 (2)**	0.007 (3)
		2.84[a]	-
$(Ag – Ag)_2$	300	2.95 (2)	0.011 (2)
	90	2.95 (2)	0.007 (3)
		2.94[a]	-
$(Ag – Ag)_3$	300	3.16 (2)	0.011 (2)
	90	3.15 (2)	0.007 (3)
		3.16[a]	-

[a] Averaged bond distances calculated from the crystal structure reported in Ref11.

To better understand the uncommon thermal behavior of $[Ag_{25}(SR)_{18}]^-$, the crystal structures of each shell within $[Ag_{25}(SR)_{18}]^-$ were reinvestigated. Remarkably, the center-Ag and $(Ag\text{-}Ag)_1$ shells form four tetrahedral units, which can be affected upon changing the temperature, as shown in Figure 6a. Similar tetrahedral units were observed in the metal core of $Au_{36}(SR)_{24}$ which also exhibits bond expansion at low temperature.[33] The tetrahedral unit has been considered as the key structure in improving the stability of Au nanoclusters having a FCC-like core. The Ag_4 tetrahedral units could serve a similar function to help stabilize the structure of $[Ag_{25}(SR)_{18}]^-$ nanoclusters. The instability of the structure caused by the staple motifs in $[Ag_{25}(SR)_{18}]^-$ can be compensated by the high stability of the metal core with tetrahedral units.

Although the $[Ag_{25}(SR)_{18}]^-$ nanoclusters have identical geometry to $Au_{25}(SR)_{18}$, they exhibit different behavior upon changing the temperature. A previous study showed that the metal core of $Au_{25}(SR)_{18}$ experiences a decrease in bond distance with decreasing temperature.[13] This is consistent with the bonding model of $Au_{25}(SR)_{18}$ shown in Figure S1, where the tetrahedral units are absent in the metal core. Thus, the tetrahedral units are unique for $[Ag_{25}(SR)_{18}]^-$. For both $[Ag_{25}(SR)_{18}]^-$ and $Au_{25}(SR)_{18}$ nanoclusters, the bonds that can change their distances are shorter than typical metallic Ag-Ag or Au-Au bonds. $[Ag_{25}(SR)_{18}]^-$ has less metallic bonds in its 13-atom core than those in $Au_{25}(SR)_{18}$. Therefore, $[Ag_{25}(SR)_{18}]^-$ shows more molecule-like behaviour than $Au_{25}(SR)_{18}$ due to the presence of the Ag_4 tetrahedral units.

In addition, longer surface-surface and staple-surface bonds ($(Ag\text{-}Ag)_2$ and $(Ag\text{-}Ag)_3$ shells) do not change in length when the temperature changes, indicating that these longer Ag-Ag bonds are insensitive to the variation of temperature. The possible reason for these unchanged bond distances is that the thiolate ligands could affect the surface-staple bonds and the longer surface-surface bonds. The surface-staple bonds are directly connected with the ligand groups, so the bond lengths cannot be changed easily. Since the long surface-surface bonds are located beneath the staple motifs (indicated by red dashed lines in Figure 6b), they are constrained by the staple motifs. The shorter surface-surface bonds, the $(Ag\text{-}Ag)_1$ shell, can expand as the temperature decreases because they are more flexible due to exposure on the surface. The surface-staple bonds and the longer surface-surface bonds are regulated by the thiolate ligands, which makes them more rigid. There exist π-π interactions between ligands (Figure S2), so the bonds that affect the orientation of the staple motifs cannot change when the temperature changes.[11] The longer surface-surface bonds can connect two staple motifs to form a ring structure as shown in Figure 6c, which makes the longer surface-surface bonds stiffer.[30] Furthermore, the four Ag-Ag

shells show larger changes in their Debye-Waller factors than the Ag-S shell, which further indicates the larger temperature effect on the Ag metal core than on the staple motifs. Therefore, varying the temperature can affect the metal core, but not the staple motifs.

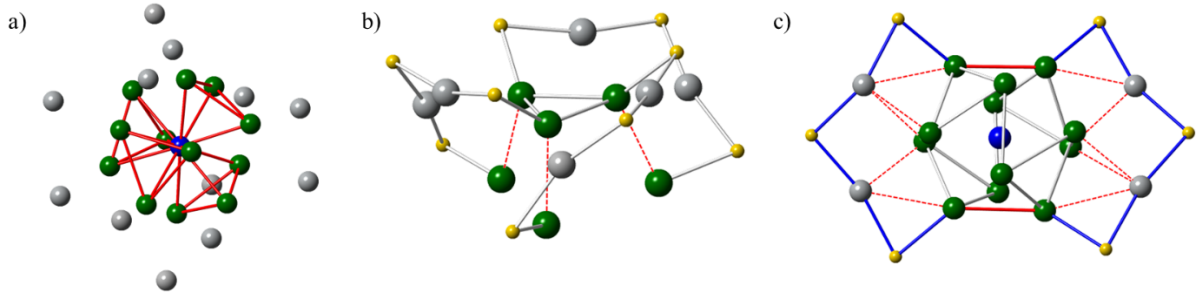

Figure 6. a) The crystal structure of $[Ag_{25}(SR)_{18}]^-$ with highlighted bonds from the first and second Ag-Ag shells. b) The partial crystal structure of $[Ag_{25}(SR)_{18}]^-$ with red dashed lines to show the long Ag-Ag bonds under beneath the staple motifs. c) The rigid ring structure in $[Ag_{25}(SR)_{18}]^-$.

4. CONCLUSIONS

In conclusion, this work demonstrated that the combination of simulated Fourier transformed extended X-ray absorption fine structure (FT-EXAFS) spectra and wavelet transformed (WT) plots was a useful approach in investigating how many EXAFS fitting shells were needed in the analysis of metal nanoclusters. It was found that the five-shell fitting method can provide more detailed and reliable information on the bonding properties of $[Ag_{25}(SR)_{18}]^-$ than the conventional two-shell fitting method. The five-shell fitting model (one Ag-S shell and four Ag-Ag shells) was successfully applied to sensitively analyze the structural changes of $[Ag_{25}(SR)_{18}]^-$ nanoclusters as the temperature varied. It was found that the 13-atom metal core of $[Ag_{25}(SR)_{18}]^-$ showed expansion as the temperature decreased. Such a negative thermal expansion behaviour, which is not commonly observed in metallic materials, could be closely related to the unique tetrahedral structural units present in the metal core. The tetrahedral structural feature in $[Ag_{25}(SR)_{18}]^-$ is in line with its more molecule-like behaviour than $Au_{25}(SR)_{18}$. Moreover, the

staple motifs and longer surface-surface bonds in $[Ag_{25}(SR)_{18}]^-$ were found to be insensitive to the change of temperature due to the rigid thiolate-metal framework. These findings provide new insights into the bonding properties of $[Ag_{25}(SR)_{18}]^-$, differing from those in other silver nanoclusters and its gold counterpart, which could be useful for its future development such as in rational design, catalytic studies, and other applications. The new EXAFS analysis method demonstrated in this work could be applied to uncover more detailed bonding properties of other small metal nanoclusters.

ASSOCIATED CONTENT

AUTHOR INFORMATION

Corresponding Authors

Peng Zhang − Department of Chemistry, Dalhousie University, Halifax, NS B3H 4R2, Canada; E-mail: peng.zhang@dal.ca

Authors

Ziyi Chen − Department of Chemistry, Dalhousie University, Halifax, NS B3H 4R2, Canada

Andrew G. Walsh − Department of Chemistry, Dalhousie University, Halifax, NS B3H 4R2, Canada

Xiao Wei − Department of Chemistry and Center for Atomic Engineering of Advanced Materials, Institute of Physical Science and Information Technology and AnHui Province Key Laboratory of Chemistry for Inorganic/Organic Hybrid Functionalized Materials, Anhui University, Hefei, Anhui 230601, P.R. China

Manzhou Zhu − Department of Chemistry and Center for Atomic Engineering of Advanced Materials, Institute of Physical Science and Information Technology and AnHui Province Key Laboratory of Chemistry for Inorganic/Organic Hybrid Functionalized Materials, Anhui University, Hefei, Anhui 230601, P.R. China

ACKNOWLEDGMENTS

The authors would like to thank the financial support from NSERC Canada. This research used resources of the Advanced Photon Source, an Office of Science User Facility operated for the US Department of Energy (DOE) Office of Science by Argonne National Laboratory, and was supported by the US DOE under contract no. DE-AC02-06CH11357, and the Canadian Light Source (CLS) and its funding partners. The CLS is supported by the CFI, NSERC, NRC, CIHR, the University of Saskatchewan, the Government of Saskatchewan, and Western Economic Diversification Canada. Z.C. would like to acknowledge the PhD Entrance scholarship from Dalhousie University and the Nova Scotia Graduate Scholarship – Doctoral. A.G.W. would like to acknowledge funding from the NSERC Post-graduate Scholarship – Doctoral and the Nova Scotia Graduate Scholarship – Doctoral.

REFERENCES

(1) Yao, Q.; Chen, T.; Yuan, X.; Xie, J. Toward Total Synthesis of Thiolate-Protected Metal Nanoclusters. *Acc. Chem. Res.* **2018**, *51*, 1338–1348.
(2) Fang, J.; Zhang, B.; Yao, Q.; Yang, Y.; Xie, J.; Yan, N. Recent Advances in the Synthesis and Catalytic Applications of Ligand-Protected, Atomically Precise Metal Nanoclusters. *Coord. Chem. Rev.* **2016**, *322*, 1–29.
(3) Zheng, K.; Yuan, X.; Goswami, N.; Zhang, Q.; Xie, J. Recent Advances in the Synthesis, Characterization, and Biomedical Applications of Ultrasmall Thiolated Silver Nanoclusters. *RSC Advances*., **2014**, *4*, 60581–60596.
(4) Shang, L.; Dong, S.; Nienhaus, G. U. Ultra-Small Fluorescent Metal Nanoclusters: Synthesis and Biological Applications. *Nano Today*. **2011**, *6*, 401–418.
(5) Yao, Q.; Wu, Z.; Liu, Z.; Lin, Y.; Yuan, X.; Xie, J. Molecular Reactivity of Thiolate-Protected Noble Metal Nanoclusters: Synthesis, Self-Assembly, and Applications. *Chem. Sci.* **2020**, *12*, 99–127.
(6) Du, X.; Jin, R. Atomically Precise Metal Nanoclusters for Catalysis. *ACS Nano* **2019**, *13*, 7383–7387.
(7) Negishi, Y. Toward the Creation of Functionalized Metal Nanoclusters and Highly Active Photocatalytic Materials Using Thiolate-Protected Magic Gold Clusters. *Bull. Chem. Soc. Jpn.* **2014**, *87*, 375–389.
(8) Yan, J.; Teo, B. K.; Zheng, N. Surface Chemistry of Atomically Precise Coinage−Metal Nanoclusters: From Structural Control to Surface Reactivity and Catalysis. *Acc Chem Res* **2018**, *51*, 17.
(9) Zhang, P. X-Ray Spectroscopy of Gold–Thiolate Nanoclusters. *J. Phys. Chem. C* **2014**, *118*, 25291–25299.

(10) Jin, R.; Zhao, S.; Xing, Y.; Jin, R. All-Thiolate-Protected Silver and Silver-Rich Alloy Nanoclusters with Atomic Precision: Stable Sizes, Structural Characterization and Optical Properties. *CrystEngComm* **2016**, *18*, 3996–4005.
(11) Joshi, C. P.; Bootharaju, M. S.; Alhilaly, M. J.; Bakr, O. M. [Ag $_{25}$ (SR) $_{18}$] $^{-}$: The "Golden" Silver Nanoparticle. *J. Am. Chem. Soc.* **2015**, *137*, 11578–11581.
(12) Desireddy, A.; Conn, B. E.; Guo, J.; Yoon, B.; Barnett, R. N.; Monahan, B. M.; Kirschbaum, K.; Griffith, W. P.; Whetten, R. L.; Landman, U. et al. Ultrastable Silver Nanoparticles. *Nature* **2013**, *501*, 399–402.
(13) MacDonald, M. A.; Chevrier, D. M.; Zhang, P.; Qian, H.; Jin, R. The Structure and Bonding of Au $_{25}$ (SR) $_{18}$ Nanoclusters from EXAFS: The Interplay of Metallic and Molecular Behavior. *J. Phys. Chem. C* **2011**, *115*, 15282–15287.
(14) Sulaiman, K. O.; Sudheeshkumar, V.; Scott, R. W. J. Activation of Atomically Precise Silver Clusters on Carbon Supports for Styrene Oxidation Reactions. *RSC Adv.* **2019**, *9*, 28019–28027.
(15) Chakroune, N.; Viau, G.; Ammar, S.; Poul, L.; Veautier, D.; Chehimi, M. M.; Mangeney, C.; Villain, F.; Fiévet, F. Acetate- and Thiol-Capped Monodisperse Ruthenium Nanoparticles: XPS, XAS, and HRTEM Studies. *Langmuir* **2005**, *21*, 6788–6796.
(16) Yamazoe, S.; Tsukuda, T. X-Ray Absorption Spectroscopy on Atomically Precise Metal Clusters. *Bull. Chem. Soc. Jpn.* **2019**, *92*, 193–204.
(17) Sharma, S.; Yamazoe, S.; Ono, T.; Kurashige, W.; Niihori, Y.; Nobusada, K.; Tsukuda, T.; Negishi, Y. Tuning the Electronic Structure of Thiolate-Protected 25-Atom Clusters by Co-Substitution with Metals Having Different Preferential Sites. *Dalton Trans.* **2016**, *45*, 18064–18068.
(18) Zhang, Z.; Walsh, A. G.; Zhang, P. Dynamic Structure of Metal Nanoclusters from Synchrotron X-Ray Spectroscopy. *J. Phys. Chem. C* **2021**, *125*, 5982–5994.
(19) Walsh, A. G.; Zhang, P. Thiolate-Protected Bimetallic Nanoclusters: Understanding the Relationship between Electronic and Catalytic Properties. *J. Phys. Chem. Lett.* **2021**, *12*, 257–275.
(20) Walsh, A. G.; Zhang, P. Thiolate-Protected Single-Atom Alloy Nanoclusters: Correlation between Electronic Properties and Catalytic Activities. *Adv. Mater. Interfaces* **2021**, *8*, 2001342–2001342.
(21) Chen, Z.; Walsh, A. G.; Wei, X.; Zhu, M.; Zhang, P. Site-Specific Electronic Properties of $[Ag_{25}(SR)_{18}]^{-}$ Nanoclusters by X-Ray Spectroscopy. *Small* **2021**, *17*, 2005162.
(22) Frenkel, A. I. Applications of Extended X-Ray Absorption Fine-Structure Spectroscopy to Studies of Bimetallic Nanoparticle Catalysts. *Chem. Soc. Rev.* **2012**, *41*, 8163–8178.
(23) Chevrier, D. M.; Conn, B. E.; Li, B.; Jiang, D. E.; Bigioni, T. P.; Chatt, A.; Zhang, P. Interactions between Ultrastable Na4Ag44(SR)30Nanoclusters and Coordinating Solvents: Uncovering the Atomic-Scale Mechanism. *ACS Nano* **2020**, *14*, 8433–8441.
(24) Shivhare, A.; Chevrier, D. M.; Purves, R. W.; Scott, R. W. J. Following the Thermal Activation of Au25(SR)18 Clusters for Catalysis by X-Ray Absorption Spectroscopy. *J. Phys. Chem. C* **2013**, *117*, 20007–20016.
(25) Lee, P. A.; Pendry, J. B. Theory of the Extended X-Ray Absorption Fine Structure. *Phys. Rev. B* **1975**, *11*, 2795–2811.
(26) Ravel, B.; Newville, M. ATHENA, ARTEMIS, HEPHAESTUS: Data Analysis for X-Ray Absorption Spectroscopy Using IFEFFIT. *J. Synchrotron Radiat.* **2005**, *12*, 537–541.

(27) Ankudinov, A. L.; Ravel, B.; Rehr, J. J.; Conradson, S. D. Real-Space Multiple-Scattering Calculation and Interpretation of X-Ray-Absorption Near-Edge Structure. *Phys. Rev. B* **1998**, *58*, 7565–7576.
(28) Kumar, R.; Sharma, G.; Kumar, M. Effect of Size and Shape on the Vibrational and Thermodynamic Properties of Nanomaterials. *J. Thermodyn.* **2013**, *1*.
(29) Funke, H.; Scheinost, A. C.; Chukalina, M. Wavelet Analysis of Extended X-Ray Absorption Fine Structure Data. *Phys. Rev. B* **2005**, *71*, 094110.
(30) Yamazoe, S.; Takano, S.; Kurashige, W.; Yokoyama, T.; Nitta, K.; Negishi, Y.; Tsukuda, T. Hierarchy of Bond Stiffnesses within Icosahedral-Based Gold Clusters Protected by Thiolates. *Nat. Commun.* **2016**, *7*, 10414.
(31) O'Day, P. A.; Rehr, J. J.; Zabinsky, S. I.; Brown, G. E. Extended X-Ray Absorption Fine Structure (EXAFS) Analysis of Disorder and Multiple-Scattering in Complex Crystalline Solids. *J. Am. Chem. Soc.* **1994**, *116*, 2938–2949.
(32) Bordiga, S.; Groppo, E.; Agostini, G.; Van Bokhoven, J. A.; Lamberti, C. Reactivity of Surface Species in Heterogeneous Catalysts Probed by in Situ X-Ray Absorption Techniques. *Chem. Rev*. **2013**, *113*, 1736–1850.
(33) Chevrier, D. M.; Chatt, A.; Zhang, P.; Zeng, C.; Jin, R. Unique Bonding Properties of the $Au_{36}(SR)_{24}$ Nanocluster with FCC-Like Core. *J. Phys. Chem. Lett.* **2013**, *4*, 3186–3191.

TOC GRAPHICS

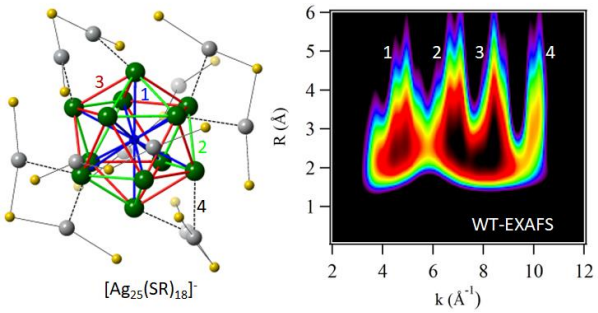

Supporting Information

New Insights into the Bonding Properties of $[Ag_{25}(SR)_{18}]^-$ Nanoclusters from X-ray Absorption Spectroscopy

Ziyi Chen[†], Andrew G. Walsh[†], Xiao Wei[‡], Manzhou Zhu[‡], Peng Zhang[,†]*

[†] Department of Chemistry, Dalhousie University, Halifax, Nova Scotia, B3H 4R2, Canada

[‡] Department of Chemistry and Center for Atomic Engineering of Advanced Materials, Institute of Physical Science and Information Technology and AnHui Province Key Laboratory of Chemistry for Inorganic/Organic Hybrid Functionalized Materials, Anhui University, Hefei, Anhui 230601, P.R. China

Corresponding Author

E-mail: peng.zhang@dal.ca

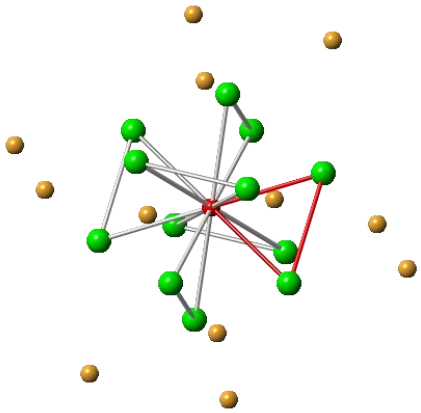

Figure S7. The crystal structure of $Au_{25}(SR)_{18}$ with the six triangular units shown.

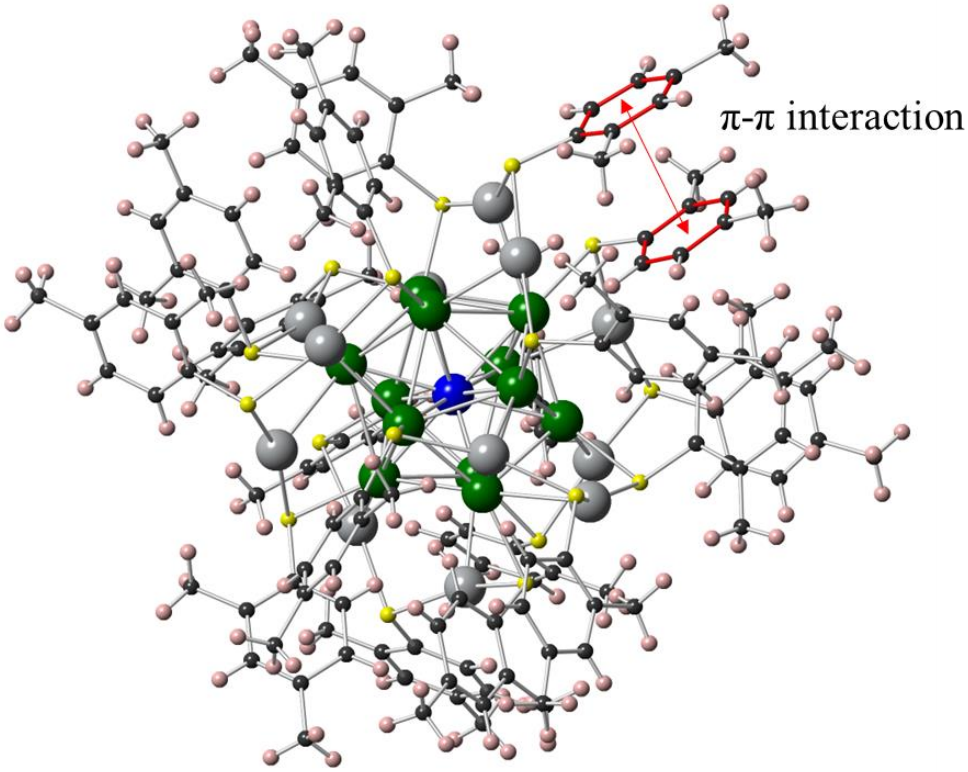

Figure S8. The crystal structure of $[Ag_{25}(SR)_{18}]^-$ with thiolate ligands to show the π-π interactions between benzene rings.